Scripta Materialia 203 (2021) 114104

Contents lists available at ScienceDirect

Scripta Materialia

journal homepage: www.elsevier.com/locate/scriptamat

Charge transfer effect on local lattice distortion in a HfNbTiZr high entropy alloy

Fanchao Meng[a,1], Wenyan Zhang[a,1], Zhukun Zhou[b], Ruixin Sheng[a], Andrew C.-P. Chuang[c], Chongchong Wu[a], Hailiang Huang[a], Shangzhou Zhang[a], Hua Zhang[a], Lilong Zhu[a,d], Liang Jiang[a], Peter K. Liaw[e], Shuying Chen[a,*], Yang Tong[a,*]

[a] Institute for Advanced Studies in Precision Materials, Yantai University, Yantai, Shandong 264005, China
[b] Institute of Laser Intelligent Manufacturing and Precision Processing, School of Mechanical Engineering, Guangxi University, Nanning, Guangxi 530004, China
[c] Argonne National Laboratory, Lemont, IL 60439, USA
[d] State Key Laboratory of Powder Metallurgy, Central South University, Changsha 410083, China
[e] Department of Materials Science and Engineering, The University of Tennessee, Knoxville, TN 37996, USA

ARTICLE INFO

Article history:
Received 2 February 2021
Revised 17 June 2021
Accepted 18 June 2021
Available online 29 June 2021

Keywords:
High-entropy alloy
Local lattice distortion
Charge transfer
Atomic pair distribution function
Reverse Monte Carlo simulation
Density functional theory

ABSTRACT

It is often assumed that atoms are hard spheres in the estimation of local lattice distortion (LLD) in high-entropy alloys (HEAs). However, our study demonstrates that the hard sphere model misses the key effect, charge transfer among atoms with different electronegativities, in the understanding of the severely distorted local structure in the body-centered cubic (BCC) HfNbTiZr HEA. Through the characterization and simulations of the local structure of the HfNbTiZr HEA, we found that the LLD regions in HfNbTiZr have larger average size compared with face-centered cubic (FCC) HEAs, but the magnitude of LLD significantly varies from one atomic site to another because of electron transfer from larger atoms, Hf and Zr, to smaller ones, Nb and Ti. Our finding may form the basis for the design of high performance HEAs through tuning their site-to-site chemical heterogeneity.

The rapid development of high entropy alloys (HEAs), solid-solution alloys consisting of multiple components at equiatomic or near-equiatomic concentration [1,2], has made discoveries of unusual edge dislocation-controlled strengthening mechanism and outstanding radiation resistance particularly in the body-centered cubic (BCC) refractory HEAs [3–5]. Compared with the most studied face-centered cubic (FCC) HEAs composed of 3*d* transition metals only [6–8], what makes refractory HEAs unique is the diverse local atomic environment caused by the large difference of electronegativity and atomic size among their constituents including 3*d*, 4*d* and 5*d* elements [9–11]. Thus, fundamental understanding of the compositional complexity effect on local atomic environments in refractory HEAs may reveal new design principles for high performance alloys.

The compositional complexity of HEAs generates local lattice distortion (LLD) since atomic size mismatch among different atomic species makes no atom occupy the perfect lattice positions. Experimental studies of local structure reveal that the FCC HEAs composed of 3d transition metals have less pronounced LLD [12,13], but some BCC refractory HEAs exhibit severe LLD with the atomic displacements even meeting the Lindemann melting criterion [11,14–16], leading to a significant improvement of yield strength [17]. Beside LLD, the compositional complexity can induce charge transfer among atomic species with different electronegativity. However, less attention has been paid to the importance of the local chemistry difference in HEAs. Compared with the most studied FCC HEAs consisting of only 3*d* transition metals, charge transfer effect (CTE) in the BCC refractory HEAs composed of 3*d*, 4*d* and 5*d* elements can be significant owing to the large electronegativity difference. The inclusion of CTE in local atomic environment study is critical for the understanding of BCC refractory HEAs' unusual mechanical behaviors and excellent radiation resistance because defects' movement can be profoundly impacted by biased CTE among elements with different electronegativity.

In compositionally complex HEAs, LLD and CTE are inevitably intertwined to diversify local atomic environments. To deeply understand this uniqueness of diversified local atomic environments in HEAs, we examined the influence of CTE on LLD in the most

* Corresponding author.
E-mail address: sychen@ytu.edu.cn (S. Chen).
[1] F. Meng and W. Zhang contribute equally to this work.

https://doi.org/10.1016/j.scriptamat.2021.114104
1359-6462/

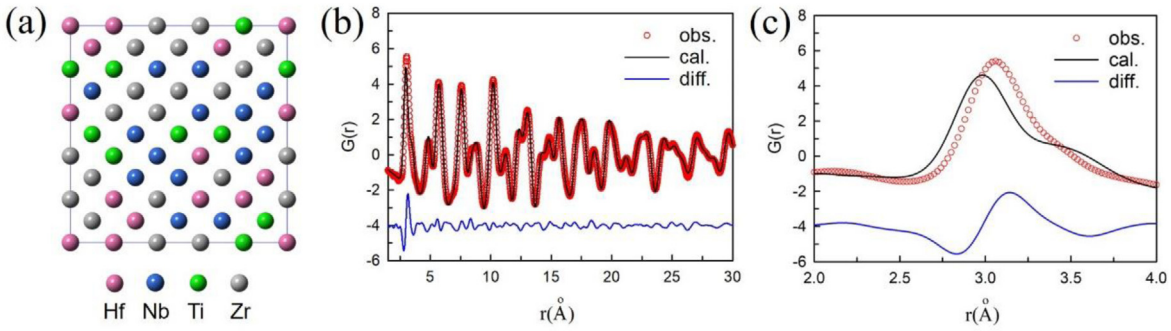

Fig. 1. (a) SQS supercell with an ideal BCC crystal structure. (b) ideal structure fit to the PDF of HfNbTiZr. (c) Close view of the fitting of the first and second PDF peaks in (b).

studied BCC refractory HEA, HfNbTiZr, through a combination of local structure characterization and different simulation methods in the present work. Our study clearly revealed that the CTE plays a critical role in the reduction of average atomic size mismatch in the HfNbTiZr HEA with severe LLD. Moreover, our finding of local environment-dependent CTE highlights another tuning parameter for the design of high performance HEAs.

The HfNbTiZr sample was prepared by arc melting Hf, Nb, Ti, and Zr metals ($\geq$ 99.5 wt% purity). The arc-melted button was flipped and remelted five times before dropping cast into a rectangular copper mold. The drop-cast ingot was then sealed into a vacuum quartz tube and homogenized at 1,473 K for 24 h, followed by water quenching. Some powder was ground from the homogenized specimen for the X-ray total scattering experiment. The total scattering measurements were conducted at the 11-ID-B beamline of the Advanced Photon Source with an X-ray energy of 58.6 keV (λ = 0.2116 Å). The PDFgetX3 [18] was used to obtain the atomic pair distribution function (PDF) by a Fourier transformation of the measured total scattering structure function, $S(Q)$,

$$G(r) = \frac{2}{\pi}\int_0^Q [S(Q)-1]\sin(Qr)dQ.$$

Here, Q is the scattering vector and r the real-space interatomic distance. The Q range for the Fourier transformation is 20 Å^{-1}. To find the atomic configuration solution for the HfNbTiZr HEA, we used both a small box modeling software, PDFgui [19], and a large box modeling software, RMCprofile [20] software to fit the measured PDF. Specifically, PDFgui was employed to fit the smallnon-distorted and relaxed supercells constructed based on the special quasi-random structure (SQS) approach to the experimental PDF by optimizing parameters including lattice constant, thermal factor, and instrument parameters. For the large Reverse Monte Carlo (RMC) structure model, RMCprofile software was used for the fitting by optimizing atomic position and instrument parameters.

To examine the LLD in HfNbTiZr, a non-distorted BCC structure model with randomly distributed Hf, Nb, Ti and Zr atoms shown in Fig. 1a was fitted to the experimental PDF over an interatomic distance range of 30 Å. Here, the non-distorted supercell containing 250 atoms was constructed, utilizing the SQS approach [21]. Fig. 1b compares the experimental and fitted PDFs by showing their difference curve. The difference curve indicates that the first and second PDF peaks cannot be fitted by the non-distorted SQS model while beyond these two PDF peaks, the experimental PDF agrees well with the fitted one, demonstrating the deviation of the local structure from the average structure. Details about the deviation can be seen from a close view of the local structure fitting, as shown in Fig. 1c. It can be seen that the first and second peaks of the experimental PDF shift towards each other to form a broad atomic shell. In other words, the average inter-atomic distance among the first nearest neighboring atoms (1NNA) increases, while the second nearest neighboring atoms (2NNA) shorten their average distance. These features demonstrate that the LLD in HfNbTiZr has a correlation length of 4 Å up to the second atomic shell, namely the average radius of the LLD regions. The correlation length reported for the FCC HEAs including CoCrFeNiPd composed of 3*d* and 4*d* transition metals is less than 3 Å, strongly localized within the first atomic shell. Compared with the FCC HEAs, the large LLD regions in the HfNbTiZr can make dislocations propagate across a rugged landscape, leading to a pronounced strengthening effect.

To explore the possible structural configuration in HfNbTiZr, we firstly implemented a RMC method, a hard sphere approach, to reproduce the experimental PDF [21]. Note that CTE was not considered in the RMC method. In the RMC fitting, a large simulation box with 21,296 atoms arranged in a random fashion was constructed first (see Fig. S1 in the supplementary file). The benefit of constructing such a large simulation box is to sample all possible local atomic environments, which must be considered for the compositionally complex HEAs. In the RMC fitting procedure, atoms were allowed to translate a random distance but without atom swap moves. Hence, the random-alloy configuration was maintained. The RMC structure model and its fit to the experimental PDF were shown in Fig. 2. The RMC structure model unambiguously reveals that atoms in the HfNbTiZr HEA displace from their BCC crystallographic sites. Meanwhile, the RMC fit matches the measured PDF very well over the whole r range, suggesting the structure model obtained from the RMC method can reproduce both the average and local structures. Moreover, another RMC fitting by allowing atoms both translate a random distance and swap equally with each other was performed to see if chemical ordering contributes to the LLD. To quantify the chemical ordering, we used the Warren-Cowley short-range order (SRO) parameter [22],

$$\alpha_n^{ij} = 1 - \frac{P_n^{ij}}{C_j}$$

where P_n^{ij} describes the probability of finding an atom of type j adjacent to an atom of type i, the subscript n refers to the nth atomic shell, and C_j is the concentration of atom j. The case of an ideal random alloy has a Warren-Cowley parameter of zero. A positive value of α_n^{ij} represents an ordered structure, while a negative value reflects chemical segregation. Our calculation shows that the inclusion of swap move introduces some Nb-Nb segregation (Fig. S2), but the fitting is not improved by the Nb-Nb segregation (Fig. S3). It is apparent that the local Nb-Nb segregation has negligible influence on the severe LLD in HfNbTiZr HEA. Therefore, the severe LLD found in the HfNbTiZr HEA is purely attributed to the atomic displacements induced by size mismatch among constituents.

We further conducted the density functional theory (DFT) calculation to examine the CTE on the LLD of the HfNbTiZr HEA. The DFT calculations were carried out by using the VASP code with the projector augmented wave method [23,24]. The exchange-

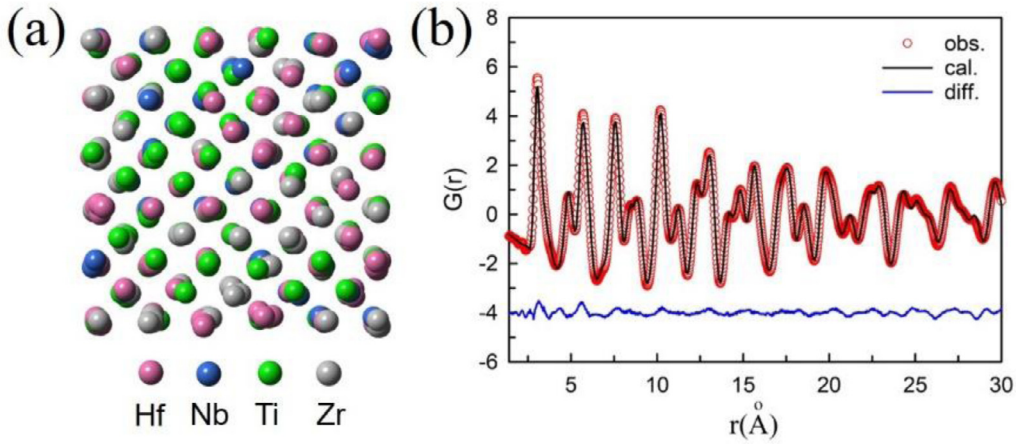

Fig. 2. (a) Structure model obtained from the RMC fit. (b) RMC fit to the PDF of HfNbTiZr. Here, only a small portion of atoms in the RMC simulation box are shown to clearly demonstrate LLD.

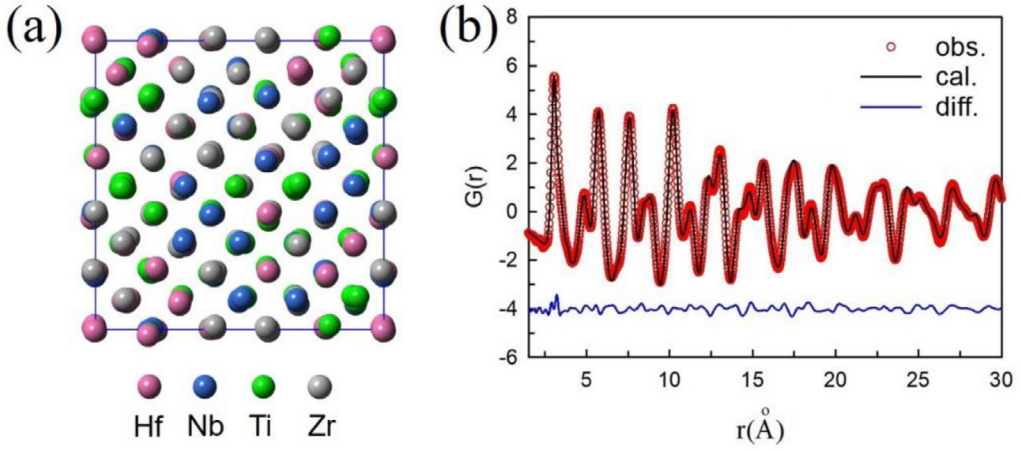

Fig. 3. (a) Relaxed supercell obtained from DFT calculation. (b) Relaxed structure fit to the experimental PDF of HfNbTiZr.

correlation functional was chosen as the generalized gradient approximation in the Perdew-Burke-Ernzerhof form [25]. A 2 × 2 × 2 Γ-centered *k*-point mesh was chosen for the Brillouin Zone sampling. The plane-wave energy cutoff was 300 eV. The energy and force tolerance were 10^{-4} eV and 0.01 eVÅ^{-1}, respectively. The non-distorted SQS supercell shown in Fig. 1a was used for the DFT calculations. The DFT simulations were performed to find the optimal volume with the lowest energy and then to relax the atomic positions by fixing the supercell volume.

Fig. 3a shows a relaxed random structure from the DFT calculation. Similar to the RMC simulation case, atoms in this relaxed supercell also displace from their ideal BCC crystallographic positions. Still, it can be seen that atoms in the DFT supercell are less distorted than those in the RMC supercell presented in Fig. 2a, which is also manifested in their mean square-root displacement being 0.239 Å and 0.351 Å for DFT and RMC supercells, respectively. To test whether the DFT supercell can reproduce the experimental PDF, we further fitted the relaxed supercell to the experimental data, as shown in Fig. 3b. The fit matches the observed PDF very well, including the local structure in the small *r* range. Structural configurations generated by both RMC and DFT simuations reproduce the experimental PDF, but atoms displace much less in the DFT supercell (Fig. 3a) than the RMC supercell (Fig. 2a), suggesting a significant impact of CTE on LLD.

In the RMC simulation, atoms are assumed as hard spheres without the consideration of CTE. However, when forming alloys constituent atoms can lose or gain electrons to vary sizes according to their electronegativity difference. Fig. 4a shows the charge change of *d* (t_{2g}) orbitals, $\Delta\rho$, for each atom in the DFT supercell after the relaxation of atomic positions. Here, a positive value of $\Delta\rho$ indicates gaining electrons while a negative value means losing electrons. It can be seen that the majority of small Nb and Ti atoms attract electrons whereas large Hf and Zr atoms donate electrons. Therefore, there exists a charge transfer from large Hf and Zr atoms to small Nb and Ti ones, which is expected since Hf and Zr atoms have smaller electronegativity values than Nb and Ti atoms. As a consequence, large Hf and Zr atoms decrease their sizes while the size of small Nb and Ti atoms increases. But the extent of the atomic-size change depends on the local atomic environments, which results in the fluctuation of the atomic size for each element. Taking the Zr element as an example, Fig. 4b and c show the local configurations of the largest and smallest Zr atoms, respectively. We can see that the largest Zr atom has more like-atoms, Zr and Hf, as the 1NNAs and 2NNAs, whereas the smallest Zr atom has more unlike-atoms, such as Ti and Nb, as the 1NNAs and 2NNAs, leading to a higher CTE around the smallest Zr atom. A similar trend is also found for the local configurations of the largest and smallest Hf atoms, exhibited in Fig. 4d and e.

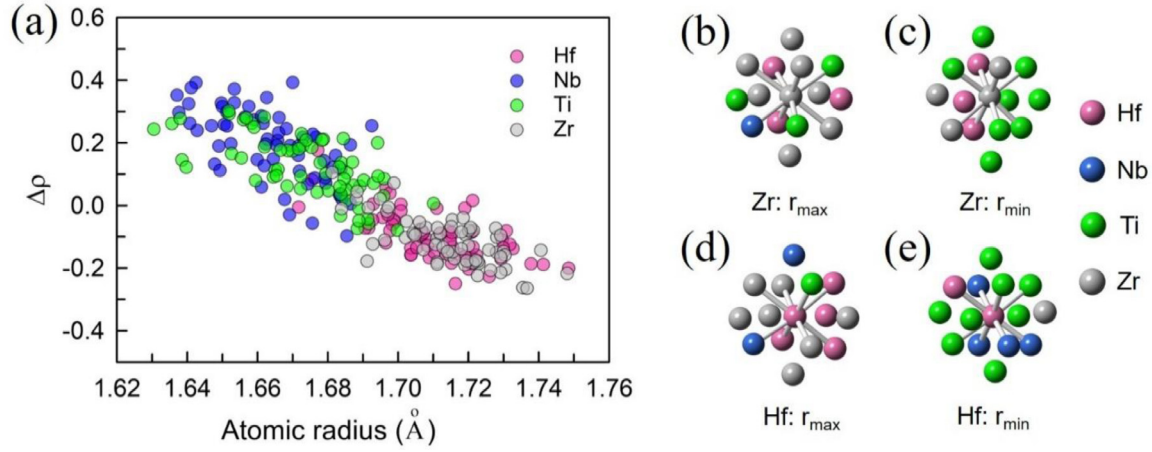

Fig. 4. (a) Correlation between charge transfer for *d* (t_{2g}) orbitals and atomic radius. (b–e) Local configurations of the largest and smallest Zr/Hf atoms.

Table 1
Charge transfer effect on atomic radii and size mismatch for the HfNbTiZr HEA.

	Atomic radius (Å)				δ (%)
	Hf	Nb	Ti	Zr	
Hard sphere	1.78	1.62	1.63	1.78	7.3
Soft sphere	1.71	1.66	1.67	1.71	1.4

A widely used parameter to describe the LLD of HEAs is the size-mismatch parameter

$$\delta = \sqrt{\sum_{i=1}^{N} c_i \left(1 - r_i / \sum_{j=1}^{N} c_j r_j\right)^2} \quad (1)$$

where N, $c_{i,j}$, and $r_{i,j}$ are the total number of constituent elements, atomic fraction, and atomic radius of the ith or jth element, respectively [26,27]. However, the CTE has been rarely considered in the LLD evaluation for HEAs by treating the constituent element with a fixed atomic size. Here, we quantitatively analyzed the CTE on the LLD of the HfNbTiZr HEA. Table 1 shows the CTE on the atomic radius for each element in the HfNbTiZr HEA. For the hard sphere case, the atomic radius, r_i, is obtained from the measured lattice constants of pure BCC metals [28] through $a^3/2 = ¾ \times \pi \times r_i^3$, where a is the lattice constant. For the soft sphere case, the atomic radius for each element is calculated from the DFT supercell through the Wigner-Seitz method [29]. It is obvious that the formation of the HfNbTiZr HEA alters the atomic radii of their constituent elements. Through charge transfer, the size mismatch is dramatically reduced from 7.3% to 1.4%, a decrease of ~80%. Therefore, the CTE reduces the extent of the average LLD in the HfNbTiZr HEA to stabilize its distorted structure. Meanwhile, we should realize that lattice distortion locally can still be very large, depending on the local environments especially where the like atoms, e.g. Zr and Hf, are neighboring to each other (Fig. 4b). The broad distribution of atomic radius for each element in Fig. 4 reflects the complexity of local atomic environments.

In summary, we investigated the LLD in the HfNbTiZr HEA through a combination of local structure characterization and simulations. The PDF analysis reveals that the local structure of the HfNbTiZr HEA deviates from its average structure by an expansion of the distance between the first nearest neighboring atoms and meanwhile a shrink of the distance of the second nearest neighboring atoms. The BCC HfNbTiZr HA has a longer LLD correlation length than all the FCC HEAs reported till now, indicating the existence of severe LLD in HfNbTiZr. The comparison between RMC and DFT simulation results demonstrates that CTE significantly reduces the average lattice distortion, but lattice distortion is still severe particularly in local regions formed by similar atoms with a negligible charge transfer effect.

Declaration of Competing Interest

There are no conflicts of interest to declare.

Acknowledgement

Y.T. acknowledges the financial support by Taishan Scholars Program of Shandong Province (tsqn202103052). S. C. acknowledges the financial support from the National Natural Science Foundation of China (No. 52001271). L. Z. acknowledges the financial support by the Taishan Scholars Program of Shandong Province (tsqn201909081) and State Key Laboratory of Powder Metallurgy (Central South University, Changsha, China). P. K. Liaw very much appreciates the supports from (1) the National Science Foundation (DMR-1611180 and 1809640) with program directors, Drs. J. Yang, G. Shiflet, and D. Farkas and (2) the US Army Research Office (W911NF-13–1-0438 and W911NF-19–2-0049) with program managers, Drs. M.P. Bakas, S.N. Mathaudhu, and D.M. Stepp. The authors appreciate Kevin Beyer's assistant in preparing the atomic pair distribution function measurement. This research used resources of the Advanced Photon Source, a U.S. Department of Energy (DOE) Office of Science User Facility, operated for the DOE Office of Science by Argonne National Laboratory under Contract No. DE-AC02-06CH11357. Extraordinary facility operations were supported in part by the DOE Office of Science through the National Virtual Biotechnology Laboratory, a consortium of DOE national laboratories focused on the response to COVID-19, with funding provided by the Coronavirus CARES Act.

Supplementary materials

Supplementary material associated with this article can be found, in the online version, at doi:10.1016/j.scriptamat.2021.114104.

References

[1] B. Cantor, I.T.H. Chang, P. Knight, A.J.B. Vincent, Mater. Sci. Eng. 375–377 (0) (2004) 213–218.
[2] J.W. Yeh, S.K. Chen, S.J. Lin, J.Y. Gan, T.S. Chin, T.T. Shun, C.H. Tsau, S.Y. Chang, Adv. Eng. Mater. 6 (5) (2004) 299–303.
[3] F. Wang, G.H. Balbus, S. Xu, Y. Su, J. Shin, P.F. Rottmann, K.E. Knipling, J.-C. Stinville, L.H. Mills, O.N. Senkov, I.J. Beyerlein, T.M. Pollock, D.S. Gianola, Science 370 (6512) (2020) 95–101.

[4] F. Maresca, W.A. Curtin, Acta Mater. 182 (2020) 235–249.
[5] O. El-Atwani, N. Li, M. Li, A. Devaraj, J.K.S. Baldwin, M.M. Schneider, D. Sobieraj, J.S. Wróbel, D. Nguyen-Manh, S.A. Maloy, E. Martinez, Sci. Adv. 5 (3) (2019) eaav2002.
[6] Z. Wu, Y. Gao, H. Bei, Acta Mater. 120 (2016) 108–119.
[7] B. Gludovatz, A. Hohenwarter, D. Catoor, E.H. Chang, E.P. George, R.O. Ritchie, Science 345 (6201) (2014) 1153–1158.
[8] Z. Wu, H. Bei, F. Otto, G.M. Pharr, E.P. George, Intermetallics 46 (0) (2014) 131–140.
[9] Y. Tong, S. Zhao, H. Bei, T. Egami, Y. Zhang, F. Zhang, Acta Mater. 183 (2020) 172–181.
[10] O.N. Senkov, G.B. Wilks, D.B. Miracle, C.P. Chuang, P.K. Liaw, Intermetallics 18 (9) (2010) 1758–1765.
[11] G.D. Samolyuk, Y.N. Osetsky, G.M. Stocks, J.R. Morris, Phys. Rev. Lett. 126 (2) (2021) 025501.
[12] Y. Tong, K. Jin, H. Bei, J.Y.P. Ko, D.C. Pagan, Y. Zhang, F.X. Zhang, Mater. Des. 155 (2018) 1–7.
[13] Y. Tong, G. Velisa, S. Zhao, W. Guo, T. Yang, K. Jin, C. Lu, H. Bei, J.Y.P. Ko, D.C. Pagan, Y. Zhang, L. Wang, F.X. Zhang, Materialia 2 (2018) 73–81.
[14] W. Guo, W. Dmowski, J.-Y. Noh, P. Rack, P.K. Liaw, T. Egami, Metall. Mat. Trans. A 44 (5) (2013) 1994–1997.
[15] C. Lee, G. Song, M.C. Gao, R. Feng, P. Chen, J. Brechtl, Y. Chen, K. An, W. Guo, J.D. Poplawsky, S. Li, A.T. Samaei, W. Chen, A. Hu, H. Choo, P.K. Liaw, Acta Mater. 160 (2018) 158–172.
[16] H. Song, F. Tian, Q.-M. Hu, L. Vitos, Y. Wang, J. Shen, N. Chen, Phys. Rev. Mater. 1 (2) (2017) 023404.
[17] C. Lee, Y. Chou, G. Kim, M.C. Gao, K. An, J. Brechtl, C. Zhang, W. Chen, J.D. Poplawsky, G. Song, Y. Ren, Y.-C. Chou, P.K. Liaw, Adv. Mater. 32 (49) (2020) 2004029.
[18] P. Juhás, T. Davis, C.L. Farrow, S.J. Billinge, J. Appl. Crystallogr. 46 (2) (2013) 560–566.
[19] C.L. Farrow, P. Juhas, J.W. Liu, D. Bryndin, E.S. Božin, J. Bloch, P. Th, S.J.L. Billinge, J. Phys. Condens. Matter 19 (33) (2007) 335219.
[20] M.G. Tucker, D.A. Keen, M.T. Dove, A.L. Goodwin, Q. Hui, J. Phys. Condens. Matter 19 (33) (2007) 335218.
[21] A. Zunger, S.H. Wei, L.G. Ferreira, J.E. Bernard, Phys. Rev. Lett. 65 (3) (1990) 353–356.
[22] J. Cowley, Phys. Rev. 77 (5) (1950) 669.
[23] G. Kresse, J. Furthmüller, Comput. Mater. Sci. 6 (1) (1996) 15–50.
[24] P.E. Blöchl, Phys. Rev. B 50 (24) (1994) 17953–17979.
[25] J.P. Perdew, K. Burke, M. Ernzerhof, Phys. Rev. Lett. 77 (18) (1996) 3865–3868.
[26] Y. Zhang, Y.J. Zhou, J.P. Lin, G.L. Chen, P.K. Liaw, Adv. Eng. Mater. 10 (6) (2008) 534–538.
[27] Y.F. Ye, Q. Wang, J. Lu, C.T. Liu, Y. Yang, Mater. Today 19 (6) (2016) 349–362.
[28] J.F. Ziegler, J.P. Biersack, U. Littmark, The Stopping and Range of Ions in Solids, 1985 Pergamon.
[29] E. Wigner, F. Seitz, Phys. Rev. 43 (10) (1933) 804–810.